

SCIENTIFIC REPORTS



OPEN

Transfer of monolayer TMD WS₂ and Raman study of substrate effects

Received: 20 September 2016

Accepted: 17 January 2017

Published: 21 February 2017

Jerome T. Mlack^{1,*}, Paul Masih Das^{1,*}, Gopinath Danda^{1,2,*}, Yung-Chien Chou^{1,3}, Carl H. Naylor¹, Zhong Lin^{4,5}, Néstor Perea López^{4,5}, Tianyi Zhang⁶, Mauricio Terrones^{4,5,6,7}, A. T. Charlie Johnson¹ & Marija Drndić¹

A facile transfer process for transition metal dichalcogenide WS₂ flakes is reported and the effect of the underlying substrate on the flake properties is investigated using Raman spectroscopy. The flakes are transferred from their growth substrate using polymethyl methacrylate (PMMA) and a wet etch to allow the user to transfer the flakes to a final substrate using a microscope and micromanipulator combined with semi-transparent Kapton tape. The substrates used range from insulators such as industry standard high-k dielectric HfO₂ and “green polymer” parylene-C, to conducting chemical vapor deposition (CVD) grown graphene. Raman spectroscopy is used first to confirm the material quality of the transferred flakes to the substrates and subsequently to analyze and separate the effects arising from material transfer from those arising from interactions with the substrate. We observe changes in the Raman spectra associated with the interactions between the substrates in the flakes. These interactions affect both in-plane and out-of-plane modes in different ways depending on their sources, for example strain or surface charge. These changes vary with final substrate, with the strongest effects being observed for WS₂ transferred onto graphene and HfO₂, demonstrating the importance of understanding substrate interaction for fabrication of future devices.

Two dimensional transition metal dichalcogenide (TMD) materials are an important addition to the two-dimensional material family as they fill in the gap between conducting graphene and insulating boron nitride. Monolayer tungsten disulfide (WS₂) in particular, with a direct band gap of 2.1 eV¹, is interesting due to its predicted strong spin orbit coupling in the single layer^{2,3} and potential for use in optoelectronics with a measured photoluminescence that is stronger than MoS₂^{4,5}.

Each of these applications will require the use of different substrates that have the potential to enhance or degrade the native properties of the WS₂ flakes. It has been shown in graphene^{3,6–8} and MoS₂^{8–14} that the device substrate and capping oxides can have an effect on the material properties, including strengthening the spin-orbit interaction³, enhancing transport properties¹¹, and tuning the band gap^{7,9,14}. One powerful method for probing changes in material properties is by analyzing shifts in the phonon peaks of the material's Raman spectrum^{5–7,9,10,12,13,15–28}. The shifts in the Raman spectrum come from sources such as interface effects which create stress and strain^{7,8,10,13,15–18,21–26,29} or charge doping^{5,19,20}, and defects^{27,28}. In the case of WS₂ layered on MoS₂^{13,21}, for example, interlayer coupling can occur and is observable as shifts and enhancements in the out-of-plane Raman modes and in the photoluminescence. The interlayer coupling also alters the band alignment between the two materials, further tuning the optical and electrical properties of the MoS₂-WS₂ heterojunction³⁰.

In previous studies, Raman spectra have been measured of WS₂ on substrates such as SiO₂^{5,15,16,20,24,31–43}, polyethylene terephthalate²⁴, Al₂O₃¹⁹, sapphire^{15,39}, boron nitride^{18,25,44}, graphene¹⁸, MoS₂^{13,21}, and quartz⁴¹.

¹Department of Physics and Astronomy, University of Pennsylvania, Philadelphia, Pennsylvania 19104, USA.

²Department of Electrical and Systems Engineering, University of Pennsylvania, Philadelphia, Pennsylvania 19104, USA.

³Department of Materials Science and Engineering, University of Pennsylvania, Philadelphia, Pennsylvania 19104, USA.

⁴Department of Physics, The Pennsylvania State University, University Park, Pennsylvania 16802, United States.

⁵Center for 2-Dimensional and Layered Materials, The Pennsylvania State University, University Park, Pennsylvania 16802, United States.

⁶Department of Materials Science and Engineering, The Pennsylvania State University, University Park, Pennsylvania 16802, United States.

⁷Department of Chemistry, The Pennsylvania State University, University Park, Pennsylvania 16802, United States.

*These authors contributed equally to this work.

Correspondence and requests for materials should be addressed to M.D. (email: drndic@physics.upenn.edu)

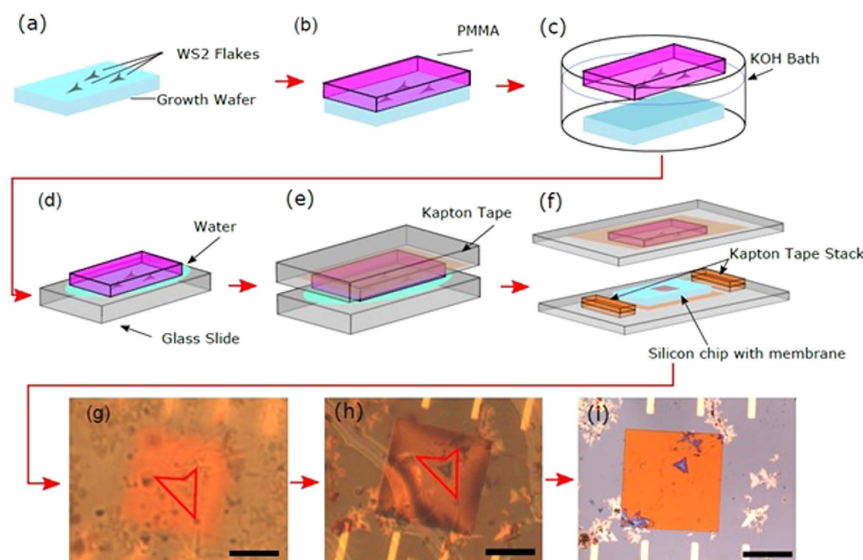


Figure 1. Diagram and optical images of a flakes transfer process. (a) WS₂ flakes are grown on a SiO₂ surface. (b) PMMA is spun onto the WS₂ growth substrate. (c) The substrate with PMMA resist is placed into 1 M KOH heated to 70 °C which dissolves the SiO₂ allowing the PMMA/flakes to be released to float on the surface of the KOH. (d) Using a glass slide the floating PMMA is removed from the KOH and transferred to a water bath for 30 minutes and then again, using a glass slide, is removed from the water and allowed to float on top of the glass slide. (e) A glass slide with double-sided Kapton tape is placed and pressed over the floating PMMA to secure it to the tape. (f) The glass slide with the PMMA is aligned over a target substrate secured to a separate glass slide and has two Kapton tape pillars that attach the two slides together upon contact. (g) The desired flake during alignment is visible under the optical microscope through the glass, tape, and PMMA and is outlined in red. A micromanipulator is used to move the flake to the desired position, with a Si₃N₄ window in the background. (h) The flake has been lowered onto the sample and pressure has been applied to secure the two slides together, providing good contact between the flake and the final substrate surface, as evidenced by the substrate surface and flake being in the same focal plane. (i) Si₃N₄ window and placed flake post overnight Acetone bath. All scale bars are 40 microns.

However, the previous studies primarily used the Raman spectra just to confirm the presence of hexagonal WS₂ by roughly locating the peaks at the expected positions, but did not look closely for any variations in the peaks owed to substrate effects or changes in the material quality. One exception, L. Su *et al.*¹⁵, looked at two types of substrates, SiO₂ and sapphire, however it focused largely on the differences in Raman shifts between as-grown structures. Currently, no experimental study of variations in the Raman spectra of WS₂ from transfer to a large number of substrate types has been reported, to our knowledge. In MoS₂ and WSe₂¹⁴, the choice of substrate has in fact been shown to have a significant impact on the Raman and thus properties of the material, further motivating our study of these effects on WS₂.

In this study, facilitated by an easy and fast transfer method, we present a focused study on the effects of transfer and substrates on the resulting material properties as determined with Raman spectroscopy. We demonstrate a flake transfer and positioning method based on previously published methods^{32,37,44–50}. Our method is most similar to that used for graphene by Zomer *et al.*⁴⁸, but uses a polymethyl methacrylate (PMMA) capping layer and potassium hydroxide (KOH) etch to remove the WS₂ from the growth substrate and Kapton tape, which leaves minimal residue and loses its adhesion in acetone, as the tape sticking the PMMA to a glass slide. The Kapton tape also serves a dual purpose in helping to create a transfer assembly which secures the location and surface contact of the PMMA/flakes to the final substrate, resulting in a transfer success rate above 84 percent for flakes transferred for this study (44 of 52 flakes), and with a single flake positioning accuracy of <10 microns, without needing a heated microscope stage^{47–49}. To understand the effect of substrate we use a variety substrates of interest for nanofabrication, specifically SiO₂, glass slides, HfO₂, graphene, and parylene-C. By comparing the location, full width at half maximum (FWHM), and amplitudes of both in-plane and out-of-plane Raman modes, before and after transfer and after a subsequent annealing step, we are able to analyze and empirically separate the effects arising from material transfer from those arising from interactions with the substrate on the phonon characteristics of monolayer WS₂.

Results

The transfer process, shown in Fig. 1, combines aspects of previous methods, used for both WS₂ and other two dimensional materials, with some new aspects. The previously reported aspects are specifically the etching of SiO₂^{32,37,45,46} to remove the flakes from the growth substrate and the use of micromanipulation of flakes on PMMA under a microscope^{44,47–50}. The flakes are CVD grown on a SiO₂/Si graphics, Fig. 1(a), as described in the Methods section. They are isolated from the growth substrate by spin coating PMMA, Fig. 1(b), and etching away the

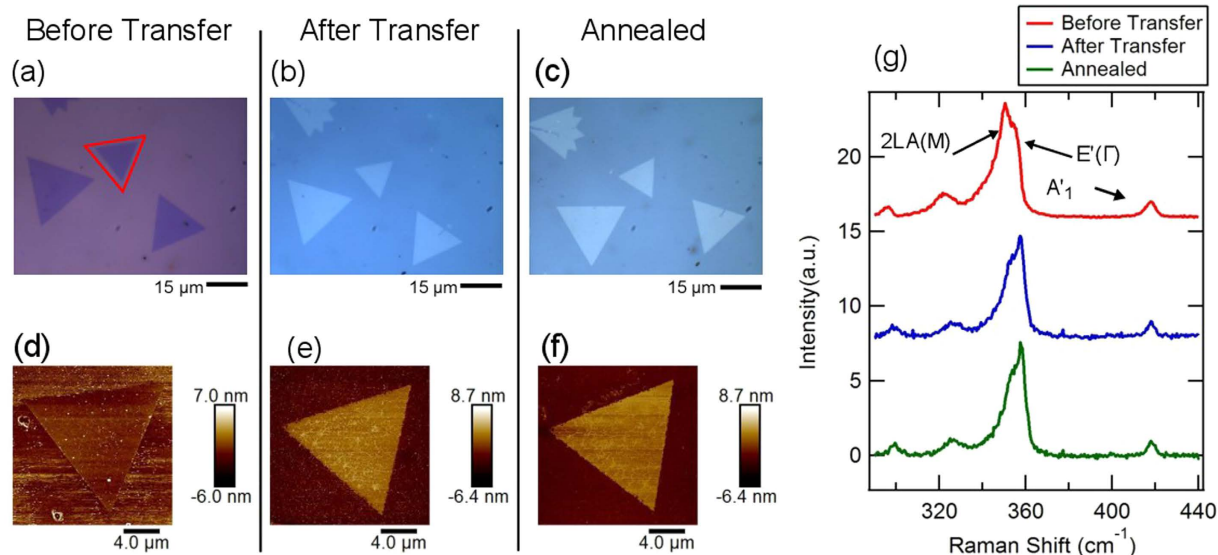


Figure 2. Optical and AFM images, with associated Raman spectra, for a monolayer WS₂ flake before and after transfer. (a) Optical image of flake, pre-transfer, on growth substrate. (b) AFM image of flake in (a) before transfer. (c) Raman spectrum of flake in (a) showing the characteristic WS₂ peaks at 351, 356, and 417 cm⁻¹. (d) Optical image of flake post transfer, on the silicon oxide substrate. (e) AFM of flake in (d). (f) AFM image of the transferred flake in (d) showing the same characteristics peaks as in (c). (g) Raman spectra of the flake before transfer (red), after transfer (blue), and after annealing (green). The Raman spectra show characteristic peaks at 351, 356, and 417 cm⁻¹. The x-axis is Raman Shift (cm⁻¹) from 320 to 440. The y-axis is Intensity (a.u.) from 0 to 20. The peaks are labeled 2LA(M), E'(Γ), and A'₁.

silicon oxide with 1 M KOH over a period of 2 hours, Fig. 1(c). The etching is followed by washing the PMMA/flakes of residual KOH in an H₂O bath, and finally they are lifted out of H₂O to float on water on a glass slide (Fig. 1(d)), flakes facing down. Where the process begins to differ from previous methods is the use of double sided Kapton tape on a separate glass slide to pick up the PMMA/flakes from the glass slide, Fig. 1(e).

The final substrate for transfer is attached to a separate glass slide with double-sided Kapton tape, and two stacks of double-sided Kapton tape with the same total thickness as the substrate are placed on either side of it as depicted in the bottom of Fig. 1(f). This assembly is placed on and centered under a microscope. Next, the PMMA/flake slide is attached, facing downwards, to a plastic arm which is then installed on a micro-manipulator stage and positioned over the substrate such that the desired flake is above the desired final position, as depicted in Fig. 1(f) and shown in the supplementary information Fig. S1.1(a–c). The microscope stage is then carefully raised. When the substrate, in this case a Si₃N₄ window, comes into focus, Fig. 1(g), adjustments to its position can be made. If the positioning is satisfactory, the substrate is raised until the surface comes into contact and is in focus with the desired flake, Fig. 1(h). The tape stacks on the sides of the chip as well as any exposed Kapton tape on the PMMA slide attach both slides together and the whole assembly can be removed from the microscope setup, supplementary information Fig. S1.1(d,e). The assembly is placed on a hot plate set to 175 °C for 20 minutes to further ensure contact, supplementary information Fig. S1.1(f). It is then allowed to cool down in air for 5 minutes and placed in an acetone bath for at least 12 hours to dissolve the PMMA, supplementary information Fig. S1.1(g). After the PMMA has been dissolved, the sample is removed, cleaned with fresh acetone and isopropanol, and dried with N₂ gas, Fig. 1(i). In order to further study the surface interaction, the sample is finally annealed under Ar:H₂ (5:1) gas mixture at 300 °C for two hours. This annealing step has been shown to be crucial in removing excess PMMA and promote surface adhesion^{9,21,51}. Specifically in the case of MoS₂⁵¹, annealing times in excess of 90 minutes are shown, via Raman and PL, to have increased the post transfer substrate bonding, creating an increased strain on the monolayer TMD.

It is important to show that the transfer method does not dramatically degrade the material. We therefore performed a detailed analysis of a monolayer flake, Fig. 2, as it went through the transfer process. The flake was transferred from the original 300 nm SiO₂/Si wafer growth substrate to a 150 nm SiO₂/Si wafer substrate. In order to check the quality of the transferred WS₂, we characterized the flake optically Fig. 2(a–c), with atomic force microscopy Fig. 2(d–f), and using Raman spectroscopy Fig. 2(g) before transfer, after transfer, and post thermal annealing. Figure 2(a–c), with a monolayer flake (bordered in red), shows that optically, there is no change in the flake throughout the transfer process. Inspection of the flakes by AFM shown in Fig. 2(d–f), indicates that some creases have formed in the flake post transfer and that the edges have been damaged by the KOH etching, but the flake is otherwise intact. The importance of the annealing step is shown in Fig. 2(f) compared to Fig. 2(e), where in Fig. 2(f) there is a marked decrease in the leftover PMMA on the surface. We therefore conclude the transfer process causes minimal damage to the flakes and that the thermal annealing is a necessary step for improving transfer quality.

The Raman data of the monolayer before transfer, shown in red as the top trace of Fig. 2(g), taken using an excitation of 532 nm with a spectrometer resolution of 0.5 cm⁻¹, shows the typical spectrum for monolayer WS₂ in range of 290 to 440 cm⁻¹ (14,35)^{15,36}. The most prominent modes that are observed in this range are the in-plane acoustic 2LA(M) at 350 cm⁻¹, in-plane optical E'(Γ) at 356 cm⁻¹, and out-of-plane optical A'₁ at 418 cm⁻¹. The

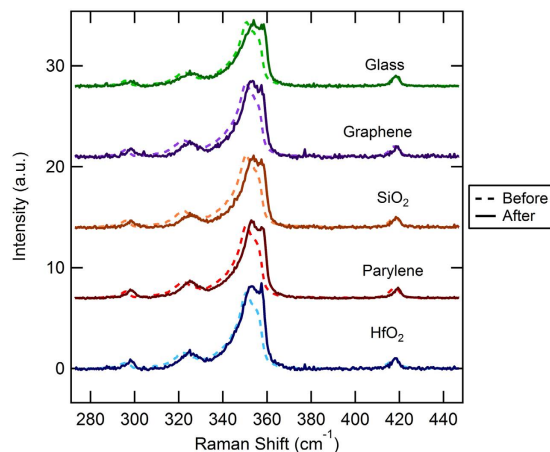


Figure 3. Raman spectra before and after transfer for each substrate type used. The spectra displayed are averaged amongst 7–11 flakes for each substrate type. For each transfer process the initial substrate was as grown on a SiO₂ substrate.

absence of the multilayer 311 cm⁻¹ Raman peak further verifies that the flake is monolayer⁴¹. The after transfer (blue) and post annealing (green) Raman spectra show a blue shift in the in-plane peaks (2LA(M) and E'(Γ)) as well as a change in the relative ratio of peak heights with the E'(Γ) peak at 356 cm⁻¹ increasing in amplitude compared to the others.

In order to investigate these changes more in depth, we have measured the Raman spectra of monolayer WS₂ transferred from its growth substrate to a range of final substrate types including 300 nm SiO₂ on silicon, 20 nm HfO₂ on 300 nm SiO₂/Si, 50 nm parylene-C on 300 nm SiO₂/Si, optically transparent glass, and graphene. For each substrate we measure the Raman spectra of several monolayer flakes before transfer, after transfer, and post annealing.

Qualitative results from the transfer process are shown in Fig. 3 which shows the averaged Raman spectra from several flakes for each substrate before transfer (on as-grown substrates) and after transfer to a new substrate (after transfer to post annealing is shown in supplementary information Fig. S2.1). The spectra are background subtracted using the adaptive baseline correction algorithm (arPLS)⁵² and normalized to the out-of-plane A₁ peak. As can be observed for all samples, there is an obvious blue shift after transfer in the in-plane modes in the 290 to 360 cm⁻¹ range and a slight blue shift in the out-of-plane A₁ peak. Qualitatively the peak heights in the 350–360 cm⁻¹ range also show an increase with the E'(Γ) peak, at 354 cm⁻¹, becoming more prominent after transfer and in one case, HfO₂, the E' peak appears to have become larger than the 2LA(M) peak.

In order to extract quantitative information from each substrate type, the spectrum for each flake transferred and measured is fit with Lorentzians in the range of 280 cm⁻¹ to 440 cm⁻¹, fitting specifically the 2LA(M)-2E''(Γ) (294 cm⁻¹), 2LA(M)-E''(Γ) (320 cm⁻¹), E'(M) (341 cm⁻¹), 2LA(M) (350 cm⁻¹), E'(Γ) (354 cm⁻¹), and A₁ (418 cm⁻¹) peaks, as by Su *et al.*¹⁵ and Gong *et al.*⁴². Results focus on analysis and comparison of the 2LA(M), E'(Γ), and A₁ peaks in terms of frequency, full width at half maximum (FWHM), and intensity ratio. The peak fitting results from each flake are averaged together for each substrate at each step, the actual fit values for each flake are provided in supplementary information Figs S3.1–S3.9. Additional plots for a sample which was not transferred, but was thermally annealed is shown in supplementary information Fig. S4.1. For all of the following plots of the averaged fit values, results before transfer are plotted in red, results after transfer in blue, and results post annealing in green.

A widely used metric for determining layer thickness is to look at the difference between the locations of the A₁ and E'(Γ) peaks^{4,34,40,41}, with the A₁ and 2LA(M) peaks showing similar behavior^{34,44}. Figure 4(a,b) show that the flakes are monolayer before annealing based on the general reported value for the separation, approximately 62.5 cm⁻¹ for A₁ to E'(Γ) and approximately 67 cm⁻¹ for A₁ to 2LA(M)³⁴. For all substrates after transfer both peak distances fall below previously reported values³⁴. Post annealing, the separation stays decreased for glass, HfO₂, and SiO₂, while for graphene and parylene-C the values increase approximately back to their initial, before transfer, value. This further indicates that a careful and comprehensive method must be used to properly identify monolayer flakes using Raman spectroscopy as discussed in A. A. Mitioglu *et al.*³⁴.

The frequencies of the Raman peaks are shown in Fig. 5 for each substrate. For all peaks analyzed there is a blue shift after transfer. As reported in previous literature^{15,18}, the overall blue shift after transfer is likely caused by a release of strain from the growth process. In comparing the peak locations to previously reported results²⁴, we infer that the flakes were likely strained up to 1.5 percent as-grown and the strain was released after transfer. The post annealing shifts are, however, more likely the result of the flake interacting with the substrate. The annealing process, as shown in the AFM images in Fig. 2d–f and supported by the literature^{9,21,51}, removes residual PMMA and water while promoting surface adhesion. Therefore, the post annealing results allow us to separate out the effects from the transfer process and analyze the substrate effects on the flakes.

For the out-of-plane A₁ peak position, which is most directly related to substrate interaction^{13,14,21,41,51}, Fig. 5(a), the peak positions post annealing show a large variation between substrates. On SiO₂, parylene-C, and

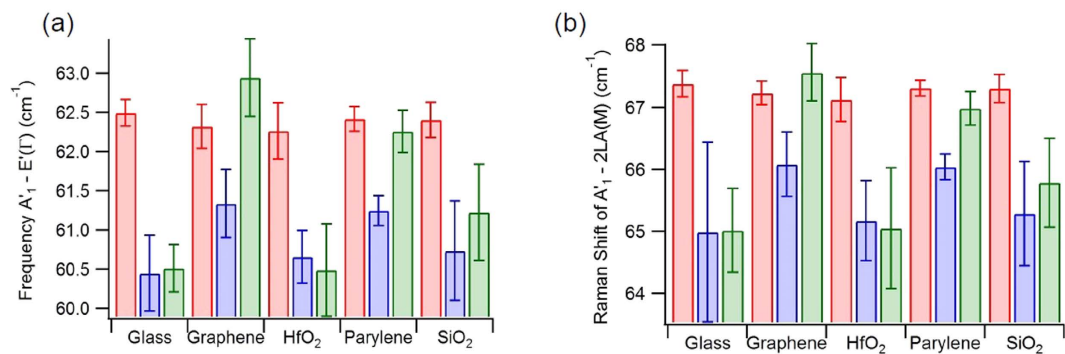


Figure 4. Bar graphs of average peak distance for WS₂ flakes on different substrates, from before (red) to after transfer (blue) and after annealing (green). (a,b) Display the average distance between the 2LA(M) to A₁' and A₁' to E'(Γ), respectively. The error presented was calculated as the standard deviation of the mean of the flake fit values for each substrate type.

graphene substrates there is a significant blue shift in the A₁' peak of approximately 1 cm⁻¹ compared to as-grown flakes. The A₁' positions for HfO₂ and SiO₂ show blue shifts after flake transfer and then return to near their original value after annealing. These shifts caused by the substrates can come from several sources including: surface charge from leftover PMMA or the surface itself, re-straining of the flakes, surface adhesion, and defects. In order to rule out some of these effects we look at the in-plane modes, which are known to be less sensitive to substrate charge and surface adhesion and primarily affected by defects and strain⁵³.

For the in-plane E'(Γ) and 2LA(M) peaks, Fig. 5(b,c) respectively, there is a large blue shift, on the order of 2 to 3 cm⁻¹ after transfer. Post annealing, the blue shift remains the same for glass, decreases to approximately 1 to 2 cm⁻¹ for HfO₂, parylene-C, and SiO₂, and goes back to near the pre-transfer value for graphene.

We can determine the likely dominant effects for these Raman peak shifts by comparing all three peaks collectively. For all substrates we rule out defects as dominant factor, as defects would introduce a red shift, not the blue shift which was observed after transfer^{27,28}. The 2LA(M) to A₁' ratio, Fig. S6.1(b), also supports this conclusion as data show a small trend of increasing ratio for each substrate after transfer as opposed to a decrease^{26,27}. For defects after annealing, we show in the supplement, Fig. S4.1, that the annealing process does not alter the peaks in as grown flakes.

In the case of the glass substrate, no new peak shifts are seen post annealing. This shows that immediately after transfer, the flakes have likely returned to an unstrained state and are unaffected by the substrate. That there is no substrate interaction, is evident from the A₁' peak which would be shifted by surface charge and adhesion. This result also suggests that any remaining PMMA from before or after annealing, likely has a minimal effect on the flakes.

For the graphene substrate, which shows a red shift for in-plane modes and a slight red shift in the A₁' peak, the flakes have likely been re-strained post annealing. This is supported by the slight increase in the FWHM of the E'(Γ), Fig. S5.1(b), which has been observed to soften and split under applied strain²⁴. Similar results have been observed on WS₂ on graphene¹⁸ using photo-luminescence (PL) measurements, where a strain related PL red shift was observed after the use of a specialized transfer method to increase surface coupling, similar to the red shift observed in our data post annealing.

HfO₂ has a small red shift in the in-plane modes, but a comparably large red shift in the out-of-plane mode. A lack of in-plane shift combined with a shift in the out-of-plane peak indicates that surface charge is the dominant factor⁵³. For parylene-C, the red shift after annealing is small, but primarily affects the in-plane modes, showing that, similar to graphene, this substrate largely re-strains the flakes. This is supported by a similar, but smaller increase in the FWHM of the E'(Γ) peak when compared to the graphene substrate. SiO₂ shows similar shifts to that observed with parylene, with the exception of the post annealing shift of the A₁', which shifts to a position near its pre-transfer location. This likely means there is some surface charge interaction. In summary, from this discussion, our empirical study indicates that we observe the largest strain interactions in graphene and parylene-C, and the largest surface charge interactions if HfO₂ and SiO₂, while in glass we observe no interactions with the substrate.

Discussion

In conclusion both a facile transfer process and the existence of a substrate effect has been shown in monolayer WS₂ flakes. The transfer process combines elements from previously published methods with the new use of Kapton tape to reduce the post transfer residue and is shown to not introduce significant defects. The changes in the Raman spectra of the flakes before, after transfer, and post annealing show the existence of in-plane strain from the growth process, the release of this strain after transfer, and the conforming of the flakes to their new substrate after the annealing process. The data for each substrate show a varying final state indicating the WS₂ flakes interact differently with each one. Graphene is the most interesting as re-straining and increases in the intensity and hardening of the in-plane mode are observed. The results highlight the importance of careful analysis of Raman data as well as the differences in substrate effects on monolayer samples, paving the way for more informed device fabrication.

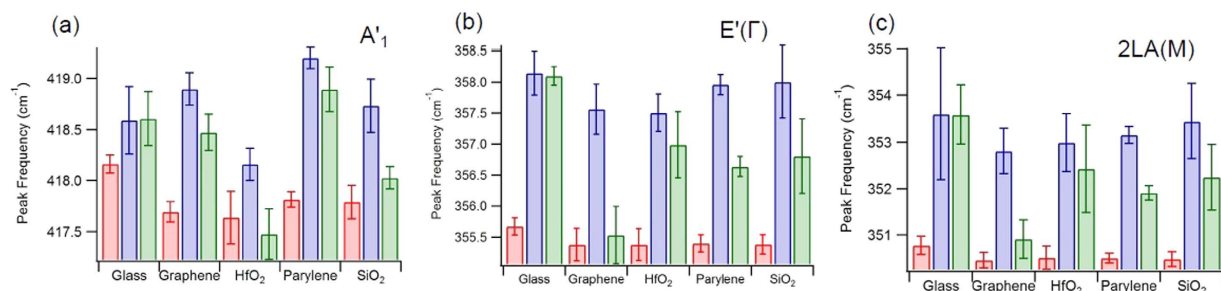


Figure 5. Bar graphs of the average peak location for WS₂ flakes on different substrates, from before (red) to after transfer (blue) and after annealing (green), for the Raman peaks studied, (a) 2LA(M), (b) E'(Γ), and (c) A'1. The error presented was calculated as the standard deviation of the mean of the flake fit values for each substrate type.

Methods

WS₂ synthesis. Monolayer and multilayer WS₂ flakes were synthesized by CVD using a method developed in a previous report⁵⁴. A 3.1 mM solution of Ammonia Metatungstate (Sigma Aldrich, 358975) and 0.02 g/mL sodium cholate is spin coated at 4000 rpm on a SiO₂/Si substrate. This chip is placed in the center of a 1 inch Lindberg Blue furnace and accompanied with a Sulfur chip placed upstream at a distance of 17 cm from previous chip. The furnace is then ramped up to 800 °C at a ramp rate of 70 °C/min. Once at 800 °C H₂ is introduced at 5 sccm for 5 min. The H₂ is then stopped and the furnace is rapidly cooled to room temperature.

Raman Measurement. Raman spectroscopy was performed in ambient conditions using a 532 nm laser excitation wavelength with a 1 μm spot size and 55 μW incident power. Spectra were obtained with an 1800 lines/mm grating attached to a NT-MDT spectrometer, resulting in a spectral resolution of 0.5 cm⁻¹.

References

- Beal, A. R. & Liang, W. Y. Excitons in 2h-wse 2 and 3r-ws 2. *Journal of Physics C: Solid State Physics* **9**, 2459, doi: 10.1088/0022-3719/9/12/029 (1976).
- Zhu, Z. Y., Cheng, Y. C. & Schwingenschlögl, U. Giant spin-orbit-induced spin splitting in two-dimensional transition-metal dichalcogenide semiconductors. *Phys. Rev. B* **84**, 153402, doi: 10.1103/PhysRevB.84.153402 (2011).
- Wang, Z. *et al.* Strong interface-induced spin-orbit interaction in graphene on ws₂. *Nature Communications* **6**, 8339, doi: 10.1038/ncomms9339 (2015).
- Gutiérrez, H. R. *et al.* Extraordinary room-temperature photoluminescence in triangular ws₂ monolayers. *Nano Letters* **13**, 3447–3454, doi: 10.1021/nl3026357 (2013).
- Peimyo, N. *et al.* Chemically driven tunable light emission of charged and neutral excitons in monolayer ws₂. *ACS Nano* **8**, 11320–11329, doi: 10.1021/nn504196n (2014).
- Wang, Y. Y. *et al.* Raman studies of monolayer graphene: The substrate effect. *The Journal of Physical Chemistry C* **112**, 10637–10640, doi: 10.1021/jp8008404 (2008).
- Ni, Z. H. *et al.* Uniaxial strain on graphene: Raman spectroscopy study and band-gap opening. *ACS Nano* **2**, 2301–2305, doi: 10.1021/nn800459e (2008).
- Wan, W. *et al.* Interlayer coupling of a direct van der waals epitaxial mos₂/graphene heterostructure. *RSC Adv.* **6**, 323–330, doi: 10.1039/C5RA22768B (2016).
- Chiu, M.-H. *et al.* Spectroscopic signatures for interlayer coupling in mos₂-wse₂ van der waals stacking. *ACS Nano* **8**, 9649–9656, doi: 10.1021/nn504229z (2014).
- Su, L., Zhang, Y., Yu, Y. & Cao, L. Dependence of coupling of quasi 2-d mos₂ with substrates on substrate types, probed by temperature dependent raman scattering. *Nanoscale* **6**, 4920–4927, doi: 10.1039/C3NR06462J (2014).
- Yu, Z. *et al.* Realization of room-temperature phonon-limited carrier transport in monolayer mos₂ by dielectric and carrier screening. *Advanced Materials* **28**, 547–552, doi: 10.1002/adma.201503033 (2016).
- Li, S.-L. *et al.* Quantitative raman spectrum and reliable thickness identification for atomic layers on insulating substrates. *ACS Nano* **6**, 7381–7388, doi: 10.1021/nn3025173 (2012).
- Zhang, J. *et al.* Observation of strong interlayer coupling in mos₂/ws₂ heterostructures. *Advanced Materials* **28**, 1950–1956, doi: 10.1002/adma.201504631 (2016).
- Yu, Y. *et al.* Engineering substrate interactions for high luminescence efficiency of transition-metal dichalcogenide monolayers. *Advanced Functional Materials* **26**, 4733–4739, doi: 10.1002/adfm.201600418 (2016).
- Su, L., Yu, Y., Cao, L. & Zhang, Y. Effects of substrate type and material-substrate bonding on high-temperature behavior of monolayer ws₂. *Nano Research* **8**, 2686–2697, doi: 10.1007/s12274-015-0775-1 (2015).
- Liu, K. *et al.* Elastic properties of chemical-vapor-deposited monolayer mos₂, ws₂, and their bilayer heterostructures. *Nano Letters* **14**, 5097–5103, doi: 10.1021/nl501793a (2014).
- Zhu, C. R. *et al.* Strain tuning of optical emission energy and polarization in monolayer and bilayer mos₂. *Phys. Rev. B* **88**, 121301, doi: 10.1103/PhysRevB.88.121301 (2013).
- Sheng, Y. *et al.* Mixed multilayered vertical heterostructures utilizing strained monolayer ws₂. *Nanoscale* **8**, 2639–2647, doi: 10.1039/C5NR06770G (2016).
- Cui, Y. *et al.* High-performance monolayer ws₂ field-effect transistors on high-κ dielectrics. *Advanced Materials* **27**, 5230–5234, doi: 10.1002/adma.201502222 (2015).
- Khalil, H. M. W., Khan, M. F., Eom, J. & Noh, H. Highly stable and tunable chemical doping of multilayer ws₂ field effect transistor: Reduction in contact resistance. *ACS Applied Materials & Interfaces* **7**, 23589–23596, doi: 10.1021/acsami.5b06825 (2015).
- Tongay, S. *et al.* Tuning interlayer coupling in large-area heterostructures with cvd-grown mos₂ and ws₂ monolayers. *Nano Letters* **14**, 3185–3190, doi: 10.1021/nl500515q (2014).

22. Conley, H. J. *et al.* Bandgap engineering of strained monolayer and bilayer mos_2 . *Nano Letters* **13**, 3626–3630, doi: 10.1021/nl4014748 (2013).
23. He, K., Poole, C., Mak, K. F. & Shan, J. Experimental demonstration of continuous electronic structure tuning via strain in atomically thin mos_2 . *Nano Letters* **13**, 2931–2936, doi: 10.1021/nl4013166 (2013).
24. Wang, Y. *et al.* Strain-induced direct–indirect bandgap transition and phonon modulation in monolayer ws_2 . *Nano Research* **8**, 2562–2572, doi: 10.1007/s12274-015-0762-6 (2015).
25. Iqbal, M. W. *et al.* High-mobility and air-stable single-layer ws_2 field-effect transistors sandwiched between chemical vapor deposition-grown hexagonal bn films. *Scientific Reports* **5**, doi: 10.1038/srep10699 (2015).
26. Xia, M., Su, Z. & Zhang, S. Raman spectra of bilayer graphene covered with poly(methyl methacrylate) thin film. *AIP Advances* **2**, doi: 10.1063/1.4739785 (2012).
27. Mignuzzi, S. *et al.* Effect of disorder on raman scattering of single-layer Mos_2 . *Phys. Rev. B* **91**, 195411, doi: 10.1103/PhysRevB.91.195411 (2015).
28. Parkin, W. M. *et al.* Raman shifts in electron-irradiated monolayer mos_2 . *ACS Nano* **10**, 4134–4142, doi: 10.1021/acsnano.5b07388 (2016).
29. Frank, O. *et al.* Compression behavior of single-layer graphenes. *ACS Nano* **4**, 3131–3138, doi: 10.1021/nn100454w (2010).
30. Gong, Y. *et al.* Vertical and in-plane heterostructures from ws_2/mos_2 monolayers. *Nature Materials* **13**, 1135–1142, doi: 10.1038/nmat4091 (2014).
31. Berkdemir, A. *et al.* Identification of individual and few layers of ws_2 using raman spectroscopy. *Scientific Reports* **3**, doi: 10.1038/srep01755 (2013).
32. Elías, A. L. *et al.* Controlled synthesis and transfer of large-area ws_2 sheets: From single layer to few layers. *ACS Nano* **7**, 5235–5242, doi: 10.1021/nn400971k (2013).
33. Kim, H.-C. *et al.* Engineering optical and electronic properties of ws_2 by varying the number of layers. *ACS Nano* **9**, 6854–6860, doi: 10.1021/acsnano.5b01727 (2015).
34. Mitioglu, A. A. *et al.* Second-order resonant raman scattering in single-layer tungsten disulfide ws_2 . *Phys. Rev. B* **89**, 245442, doi: 10.1103/PhysRevB.89.245442 (2014).
35. O'Brien, M. *et al.* Mapping of low-frequency raman modes in cvd-grown transition metal dichalcogenides: Layer number, stacking orientation and resonant effects. *Scientific Reports* **6**, doi: 10.1038/srep19476 (2016).
36. Peimyoo, N. *et al.* Thermal conductivity determination of suspended mono- and bilayer ws_2 by raman spectroscopy. *Nano Research* **8**, 1210–1221, doi: 10.1007/s12274-014-0602-0 (2014).
37. Song, J.-G. *et al.* Layer-controlled, wafer-scale, and conformal synthesis of tungsten disulfide nanosheets using atomic layer deposition. *ACS Nano* **7**, 11333–11340, doi: 10.1021/nn405194e (2013).
38. Staiger, M. *et al.* Splitting of monolayer out-of-plane A'_1 raman mode in few-layer ws_2 . *Phys. Rev. B* **91**, 195419, doi: 10.1103/PhysRevB.91.195419 (2015).
39. Xu, Z.-Q. *et al.* Synthesis and transfer of large-area monolayer ws_2 crystals: Moving toward the recyclable use of sapphire substrates. *ACS Nano* **9**, 6178–6187, doi: 10.1021/acsnano.5b01480 (2015).
40. Zeng, H. *et al.* Optical signature of symmetry variations and spin-valley coupling in atomically thin tungsten dichalcogenides. *Scientific Reports* **3**, doi: 10.1038/srep01608 (2013).
41. Zhao, W. *et al.* Lattice dynamics in mono- and few-layer sheets of ws_2 and wse_2 . *Nanoscale* **5**, 9677–9683, doi: 10.1039/C3NR03052K (2013).
42. Gong, Y. *et al.* Tellurium assisted low temperature synthesis of mos_2 and ws_2 monolayers. *ACS Nano* **9**, 11658–11666, doi: 10.1021/acsnano.5b05594 (2015).
43. McCreary, K. M. *et al.* The effect of preparation conditions on raman and photoluminescence of monolayer ws_2 . *Scientific Reports* **6**, doi: 10.1038/srep35154 (2016).
44. Withers, F., Bainton, T. H., Hudson, D. C., Craciun, M. F. & Russo, S. Electron transport of ws_2 transistors in a hexagonal boron nitride dielectric environment. *Scientific Reports* **4**, doi: 10.1038/srep04967 (2014).
45. Reina, A. *et al.* Large area, few-layer graphene films on arbitrary substrates by chemical vapor deposition. *Nano Letters* **9**, 30–35, doi: 10.1021/nl801827v (2009).
46. Liang, X. *et al.* Toward clean and crackless transfer of graphene. *ACS Nano* **5**, 9144–9153, doi: 10.1021/nn203377t (2011).
47. Dean, C. R. *et al.* Boron nitride substrates for high-quality graphene electronics. *Nature nanotechnology* **5**, 722–726, doi: 10.1038/nnano.2010.172 (2010).
48. Zomer, P. J., Dash, S. P., Tombros, N. & van Wees, B. J. A transfer technique for high mobility graphene devices on commercially available hexagonal boron nitride. *Applied Physics Letters* **99**, doi: 10.1063/1.3665405 (2011).
49. Roy, K. *et al.* Optically active heterostructures of graphene and ultrathin mos_2 . *Solid State Communications* **175–176**, 35–42, doi: 10.1016/j.ssc.2013.09.021 (2013).
50. Leon, J. *et al.* Transferring few-layer graphene sheets on hexagonal boron nitride substrates for fabrication of graphene devices. *Graphene* **3**, 25–35, doi: 10.4236/graphene.2014.33005 (2014).
51. Su, L., Yu, Y., Cao, L. & Zhang, Y. *In-situ* monitoring of thermal annealing induced evolution in film morphology and film-substrate bonding in a monolayer mos_2 film. *arXiv:1609.05077 [cond-mat.mtrl-sci]* (2016).
52. Zhang, Z.-M., Chen, S. & Liang, Y.-Z. Baseline correction using adaptive iteratively reweighted penalized least squares. *Analyst* **135**, 1138–1146, doi: 10.1039/B922045C (2010).
53. Chakraborty, B. *et al.* Symmetry-dependent phonon renormalization in monolayer mos_2 transistor. *Phys. Rev. B* **85**, 161403, doi: 10.1103/PhysRevB.85.161403 (2012).
54. Kim, M. S. *et al.* Biexciton emission from edges and grain boundaries of triangular ws_2 monolayers. *ACS Nano* **10**, 2399–2405, doi: 10.1021/acsnano.5b07214 (2016).

Acknowledgements

Z.L., N.P., T.Z., M.T. acknowledge the support from the US Army Research Office MURI grant W911NF-11-1-0362. All authors acknowledge partial support from the Penn State Center for Nanoscale Science (DMR-0820404 and DMR-1420620). We also thank the National Science Foundation for the following grants: 2DARE-EFRI-1433311 and 2DARE-EFRI-1542707.

Author Contributions

J.T.M., P.M.D., and M.D. devised experiments. J.T.M., P.M.D., and G.D. devised transfer method. J.T.M., P.M.D., G.D., and Y.-C.C. tested and refined transfer method. P.M.D. and Y.-C.C. performed sample preparation, Raman spectroscopy, and atomic force microscopy. J.T.M. analyzed Raman data and prepared all figures and results discussion. Preliminary materials grown by Z.L., N.P.L., T.Z., and M.T. with the materials analyzed in this article provided by C.H.N. and A.T.C.J. All authors contributed to the manuscript preparation.

Additional Information

Supplementary information accompanies this paper at <http://www.nature.com/srep>

Competing financial interests: The authors declare no competing financial interests.

How to cite this article: Mlack, J. T. *et al.* Transfer of monolayer TMD WS₂ and Raman study of substrate effects. *Sci. Rep.* 7, 43037; doi: 10.1038/srep43037 (2017).

Publisher's note: Springer Nature remains neutral with regard to jurisdictional claims in published maps and institutional affiliations.



This work is licensed under a Creative Commons Attribution 4.0 International License. The images or other third party material in this article are included in the article's Creative Commons license, unless indicated otherwise in the credit line; if the material is not included under the Creative Commons license, users will need to obtain permission from the license holder to reproduce the material. To view a copy of this license, visit <http://creativecommons.org/licenses/by/4.0/>

© The Author(s) 2017